32nd Congress of the International Council of the Aeronautical Sciences
September 6-10, 2021
Pudong Shangri-La, Shanghai, China

Design and Performance of a Low Fan-Pressure-Ratio Propulsion System

Rainer Schnell[1], Erik Goldhahn[2], Marc Julian[3]

[1]DLR - German Aerospace Center, Institute of Propulsion Technology, Linder Hoehe, 51147 Koeln, Germany,
rainer.schnell@dlr.de

[2]AIRBUS Operations GmbH, Aerodynamic Testing EGAXG, Airbus-Allee 1, 28199 Bremen, Germany
erik.goldhahn@airbus.com

[3]AIRBUS Operations SAS 316 route de Bayonne, P.O. BOX M0131/1, 31300 TOULOUSE Cedex 09, France
marc.julian@airbus.com

Abstract

A propulsion system, comprising of a low pressure ratio fan stage with bypass and core section and an engine representative, short intake and nacelle was designed and its aerodynamic performance was assessed over a wide range of engine and aircraft operating conditions. Since the detailed fan and intake design was carried out separately and its design intent is known and understood, an assessment of how the individual component performance was influenced by the respective coupling was possible.

The basis for all design efforts was a thermodynamic cycle derived from Single-Aisle short-medium range airliner thrust requirements over the entire flight regime and major certification points. A bypass ratio of 16 was targeted and 2025+ technology assumptions were made. This specification defined all fan operating conditions and a detailed and engine representative fan design was carried out to meet those requirements. All major design choices will be justified based on existing design expertise for aero engine fans over a wide range of application and data from open literature. Concurrently to the fan design, an ultra-short intake was designed to accommodate the large fan diameters as expected for future UHBR engines, targeting at meeting requirements such as little cross wind and angle of attack sensitivity as well as a high flow capacity. The entire propulsion system was then assessed by means of steady and unsteady CFD. Here the focus will be on typical angle of attack conditions as experienced during Take-Off at high fan power settings. The resulting unsteady interaction between the fan and the non-axisymmetric inflow, stemming from both simple kinematics due to induced swirl, as well as additional acceleration and diffusion near the upper and lower intake lip, will be discussed in detail. Furthermore, the influence of the angle of attack on maximum flow capacity of the fan will be discussed, along with an analysis of the fan presence effect on the occurrence of separation within the intake for very high values thereof. All results shown in the paper will focus on both analysing the flow physics as well as better understanding how the fan and intake design is influenced by the close coupling between a short intake and a low fan pressure ratio fan.

Keywords: UHBR Aero Engine, Fan and Intake Design, Aerodynamic Performance, Engine Integration, Angle of Attack Conditions, Unsteady Aerodynamics, CFD, Harmonic Balance Technique

1. MOTIVATION AND OBJECTIVE

Current propulsion systems for commercial transport aircraft utilize turbofan engines with a maximum bypass ratio of 9 to 12 and future engines most likely will have substantially higher bypass ratios. The fan operating in such engines will feature a lower pressure ratio and a high mass flow rate. To accommodate this high mass flow rate, the engine inlet diameters are increasing. This is associated with large diameter nacelles, which in turn become heavier and create more friction drag due to their increased wetted surface. Also, the integration of such

engines in under wing configuration becomes more challenging as the nacelles couple closer to the wing. As the diameter of the fan increases to allow for the high mass flow the speed of the fan has to decrease to limit tip speeds. This in turn has implications on the low pressure spool layout by either incorporating a gear box between the fan rotor and the rest of the low pressure spool or adapting the stage count of low pressure compressor and turbine. Both will add weight as well. To counterbalance partially these penalties, the intention is to design a significantly shorter engine air intake. This concept addresses nacelle drag and weight optimization and it will also increase intake pressure recovery and ease installation of the powerplant system on the aircraft compared to a classical length intake. But on the other hand, a short intake presents some drawbacks and challenges. The difficulty for intake to feed the engine with a good quality flow is increased and the fan is less protected from upstream flow variations (velocity distortion, residual incidence). Moreover, the area for acoustic treatment is reduced. To address the impact of an UHBR fan with a short intake on performance, integration and acoustic signature a generic propulsion system representing a next generation UHBR engine has been designed to allow for CFD and CAA investigations.

2. TOP LEVEL SPECIFICATION AND ENGINE CYCLE

The performance characteristics of the low pressure fan propulsion system have been defined on the basis of thrust requirements for a short to medium range single aisle aircraft considering a cruise bypass ratio of 16. For this target application, requirements from acoustics as well as aircraft and component performance have been used to define relevant operation points. For acoustic considerations the thrust requirements are related to the measurement points used by the airworthiness agencies for certification. An additional acoustic requirement was to restrict the relative tip Mach number at take-off to values around 1. The acoustic certification points are defined as follows:

- Fly-over: 6.5 km from the brake release point and under the take-off flight path
- Sideline: the highest noise measurement recorded at any point 450 m from the runway axis during take-off.
- Approach: 2 km from the runway threshold, under the approach flight path

Performance aspects are incorporated by selecting operation points in accordance with standard aircraft operation procedures:

- Take-off Thrust: maximum thrust available for take-off
- MCT: Maximum thrust that can be used without time limit
- CL: Maximum thrust during the climb phase
- Cruise: Typical thrust during the cruise phase of a flight

Finally an additional operation point for the investigation of the engine inlet performance has been incorporated. This point is characterized by a maximum inlet mass flow density. It is used to demonstrate inlet performance at extreme conditions regarding engine operation during take-off and has been denoted as maximum flow capacity condition (MFC). Since the propulsion system in question is a projection of a possible future engine, no component data are available. Furthermore the focus for the design and subsequent investigations is on fan performance. An in-house thermodynamic model has been used to define the fan operation conditions It is based on the thrust requirements for a typical single aisle short to medium range aircraft. Together with flight conditions and some geometric constraints, the reduced mass flow and the fan pressure ratio can be found for the cruise condition. All other operating points are derived from that fixing the nozzle cross sections in

relation to the cruise nozzle. This model also incorporates a largely simplified simulation for the core conditions (calorically perfect gas, no power off takes, no bleed or cooling air off takes). Results from the specification using the simple thermodynamic model as provided for the fan design were internally verified using the DLR cycle analysis tool GTlab [28]. The cruise condition has been used as a reference condition and with the target bypass ratio of 16 the optimal fan pressure ratio has been determined using this model, Figure 1, left). This reference point also fixes the nozzle cross sections for fan and bypass and allows deriving all other operating conditions from that (Figure 1, right). To limit the fan pressure ratio for the take-off points and the max. mass flow density point a variable area fan nozzle has been assumed. Its cross section is related to the reference point nozzle cross section. Together with some additional values on stall margins this input has been used as the basis for the fan module development.

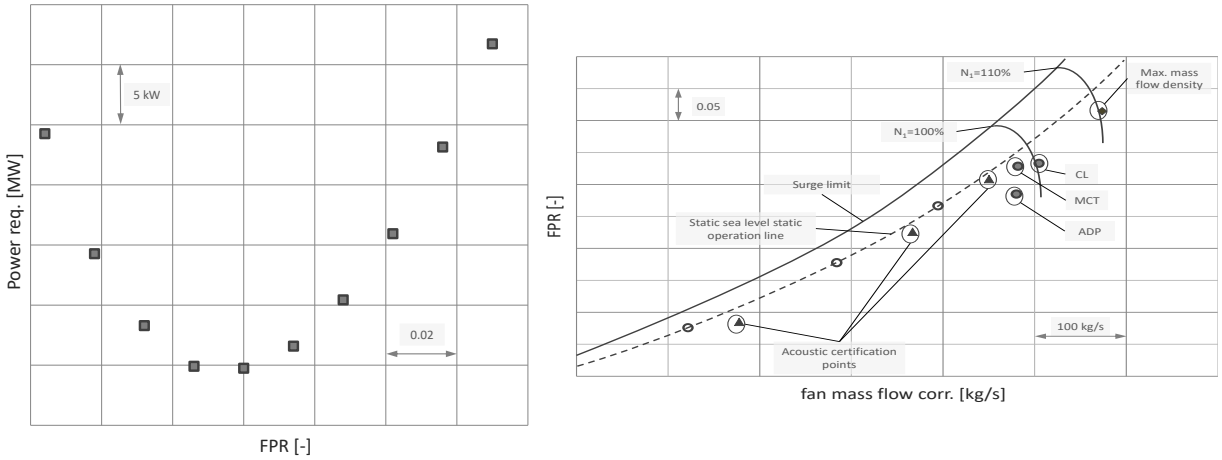

Figure 1 - Left: Optimal fan pressure ratio for the cruise condition and a bypass rate of 16. Right: operation points for the fan module design

3. FAN CONCEPTUAL DESIGN

One of the most important design choices for the fan to be made at conceptual level is fixing the blade tip speed at targeted (design) fan total pressure ratio. Typically, this choice takes into account fan performance considerations as well as restrictions imposed by the gas generator. For the current design, a geared architecture was envisioned, allowing for some flexibility in the choice of resulting tip speed of the fan at given outer diameter, without any other constraints being imposed by the core engine. The basis for choosing the (ISA-corrected) tip speed was the work coefficient in the following form:

$$\Psi = \frac{\Delta h_t}{u_{mean}^2} = \frac{2c_p T_{t0}\left(\pi_t^{\frac{\gamma-1}{\gamma}} - 1\right)}{\eta_{is}(1+\nu^2)u_{tip}^2} \approx \frac{c_{u,2,mean}}{u_{mean}}$$

For a given enthalpy rise (or total pressure ratio and fan efficiency), this parameter yields the ratio between the average change in swirl (which is caused by either flow turning or diffusion in the relative system) and the mean circumferential velocity. Low values of Ψ hence indicate higher tip velocities and lower levels of flow turning and vice versa. Typically choosing the “right” Ψ requires a careful balance between shock losses at high tip Mach number and profile losses resulting from an increased flow turning. Other aspects, such as aerodynamic stability and acoustic benefits at low tip speed and higher swirl levels, potentially causing additional destructive and hence regarding tonal noise beneficial interferences of the rotors wakes onto the OGV, also play an important role [4].

To support the choice being made for this particular configuration, existing data from internal design studies [11][12][13][15][18][22] and open literature [1][3] were taken advantage of. All those

designs, which stem from different contexts and following different design approaches and philosophies, have in common a sufficiently high level of maturity. The entire data base is shown in Figure 2 (left) by plotting (ISA corrected) blade tip speed over fan pressure ratio. Lines of constant Ψ are also shown in the figure and most designs are clustered around Ψ-values of around 0.5, indicating a favorable region for its optimal choice which seems independent of the FPR and u_{tip} (although this seems unlikely to exist universally, given the different nature of highly transonic, high-FPR fans compared with low transonic or subsonic fans at much lower FPR levels). The design realized in this study resulted in a rather high value of Ψ≈0.6, yielding a low tip speed at given FPR. This choice was mainly driven by acoustic considerations, limiting the relative inflow Mach number at the blade tip to unity (SDL), but still enabling high levels of fan efficiency. Aerodynamic stability was considered as well and a sufficiently large working range was ensured, this was however not the primary design focus due to the generic nature of the design. Another important and often critical aspect for any fan design is its flow capacity or specific mass flow rate

$$\frac{w_{red}}{A_{inlet}} = \frac{p_t}{\sqrt{T_t}}\sqrt{\frac{\gamma}{R}}\, Ma_{ff}\left(1+\frac{\gamma-1}{2}Ma_{ff}^2\right)^{-\frac{\gamma+1}{2(\gamma-1)}}$$

values of which are also shown in Figure 2 (right) for ADP as well as for typical Top-of-Climb conditions. For the given design the values thereof are similar to other designs, yielding rather identical Mach numbers at the fan face. However, an even higher flow capacity beyond common values was requested as well (see point indicated “MFC”); this requirement was mainly driven by intake considerations and needed further attention in the choice of hub-to-tip ratio, blade numbers and annulus lines in the rotor region. The number of OGV was mainly chosen by acoustic considerations ensuring a cut-off design at 1BPF and a sufficient amount of sweep was realized e.g. [4]; the chord length of the individual sections was then chosen based on maximum blade diffusion number (DF). The resulting values for DF for both, rotor and OGV are shown in Figure 3, yielding moderate levels (<0.5) in all relevant operating conditions and with maximum values close to 0.55 near the stability limit. For realizing this at given (low) values of rotor tip speed, a relatively large chord was introduced to ensure the necessary flow turning can be delivered.

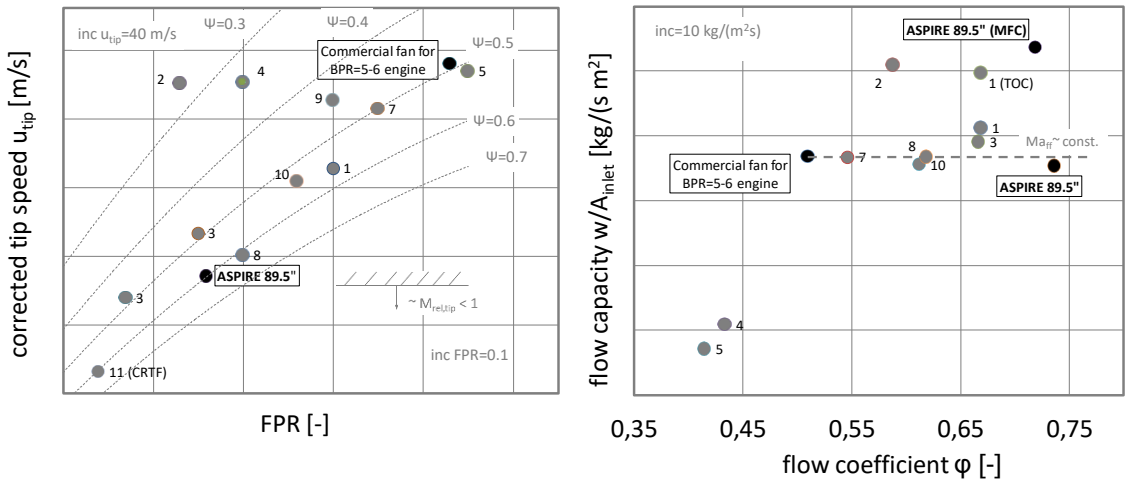

Figure 2 - Fan design parameters and classification thereof by comparison with existing (rig) designs. Left: dashed lines indicate values of constant work coefficient Ψ at constant η; Right: shown are values for specific mass flow rate - at design (cruise) conditions if not indicated otherwise - over flow coefficient φ (NB: the numbers given in the figures do not relate to the numbers given in the references whatsoever)

The final propulsor geometry resulting from the aforementioned conceptual design considerations, which was heavily supported by an in-house Throughflow approach using an

optimized airfoil data base [21] and subsequently being optimized applying a CFD/FEM based optimization approach as described in [12], is shown in Figure 4. Geometric constraints defined prior to starting the fan design ensured the seamless connection with the intake and exhaust parts as they were designed by Airbus. The aeroelastic characteristics of this propulsor are described in [22], yielding a flutter free design at acceptable static stress values (van Mises) and satisfying Campbell characteristics.

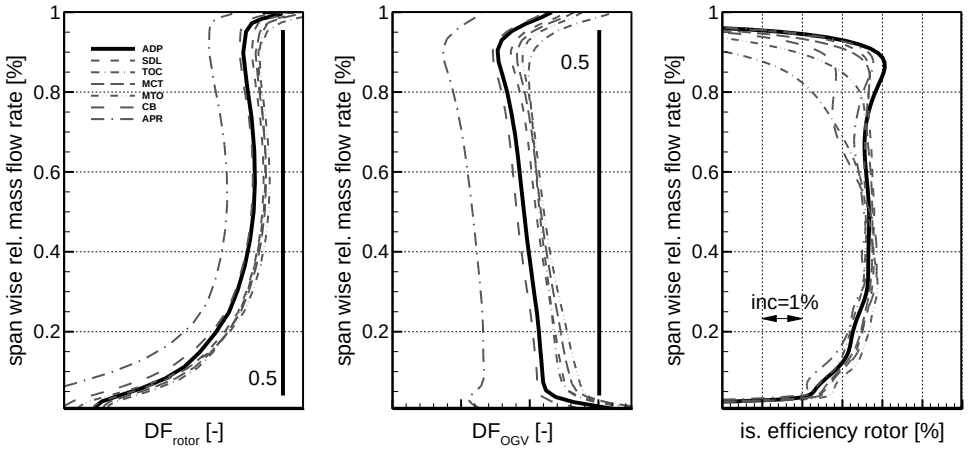

Figure 3 - Span-wise distribution of Rotor and OGV diffusion numbers (DF) and isentropic rotor efficiency in all operating conditions – Results from RANS computations as carried out during the design process

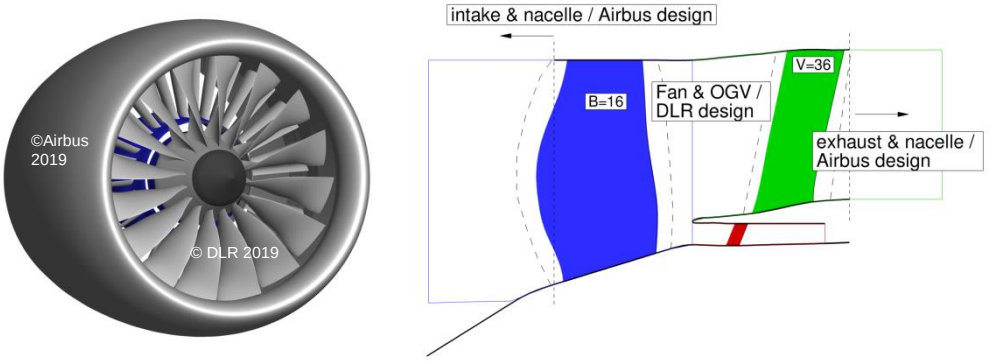

Figure 4 - Front view on the fan stage integrated in the nacelle (left) and annulus lines in the region of the fan, bypass and core section (right)

4. FAN INTAKE AND NACELLE DESIGN

As introduced in chapter 2, the intake and nacelle as designed by Airbus (see Figure 4) aim at analyzing and better understanding the fan / intake flow coupling for low L/D ratio and hence short intakes. In the current state, without fan presence effect, this design does not pretend to be fully compatible with engine and aircraft classical specifications. The intake has been designed with the target for meeting requirements such as little cross wind and angle of attack sensitivity as well as a high flow capacity. As presented in Figure 5, the short intake non-dimensional length (with regard to fan case diameter D) is L/D = 0.24. The intake length L is defined as the distance between fan blade root leading edge and intersection between intake highlight plane and engine axis. A drop angle δ of 2° has been chosen. This parameter is the angle between lower lip leading edge / upper lip leading edge direction and a plane normal to engine axis. It is classically a compromise between low-speed and high speed requirements.

The air intake has been designed based on steady-state RANS CFD computations (without any fan simulation) run with Onera-Airbus-Safran elsA software. The calculations used a structured mesh and a Spalart-Allmaras turbulence model. At maximum mass flow capacity requirement, three types of intake flow have been observed pending angle-of-attack considered: globally attached, semi-separated and deeply separated flows. The nacelle external part has been designed to be compatible with the short intake and a nozzle exit area chosen among the ones defined in the project framework to study the mass flow effect. Focusing on the interaction between fan and intake, the study presented in this paper does not require any jet flow simulation. Consequently the nozzle has not been included in the computations (as opposed to the simulations carried out in [11]) and here the jet flow was replaced by a rigid geometry. Similarly, bifurcations downstream of the fan module have not been simulated to avoid any upstream impact on the fan module and the baseline OGVs were designed without any bifurcation consideration.

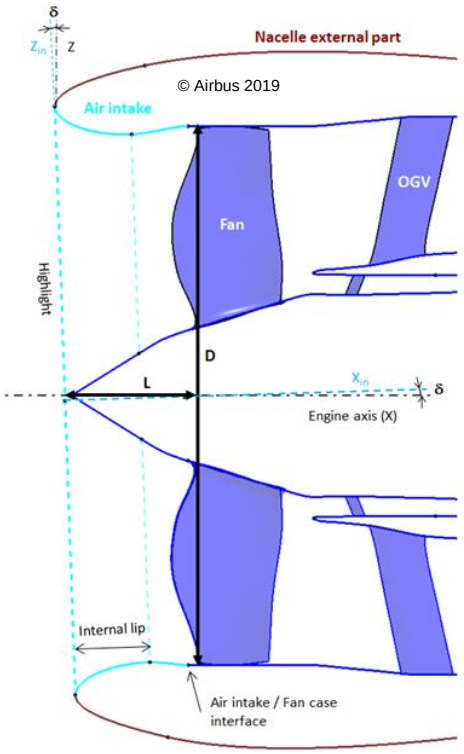

Figure 5 Short air intake geometrical characteristics

5. PERFORMANCE ASSESSMENT

5.1 Isolated Fan

As part of the overall design task, the performance of the isolated fan (without the intake) was assessed over the entire flight regime by steady state RANS simulations using DLRs TRACE CFD framework [7]. The resulting performance characteristics are shown in Figure 6 (left), together with the span wise distribution of circumferentially averaged rotor total pressure ratio (right). As intended, the ADP was located around peak efficiency and the TOC point yielded only a very small drop in stage efficiency, whilst still ensuring a positive choke margin. MTO and SDL conditions were the most demanding in terms of aerodynamic stability and remaining stall margin; their location however was controlled by taking advantage of a variable area nozzle and hence is less critical as to compared with fixed nozzle operation. Since one of the major objective of this configuration was to study acoustic effects of a UHBR engine, special attention has also been drawn to the performance near the acoustic certification points APR (not shown here) and SDL. The contours of relative Mach number as shown in Figure 7 near the blade tip show only a limited transonic regime on the suction side, terminated by a small shock in the front part of the profile at ADP conditions. At SDL conditions, which essentially is at the same corrected rotational speed, this shock is more pronounced and moves upstream due to the positive incidence and the operating point being located closed to stall. At TOC conditions the tip sections are just starting to choke with a normal shock developing in the passage. Since the lower sections of the fan are still not fully choked a positive choke margin for the fan still prevails. To assess the OGV performance in more detail the span wise distributions of the average Mach number and flow angle are plotted in Figure 8, along with the resulting isentropic Mach number at mid span (right). Over the entire range of operation, the OGV needs to cope with inlet angle variations in the order of 8° between TOC and APR at Mach number levels varying by 0.4.

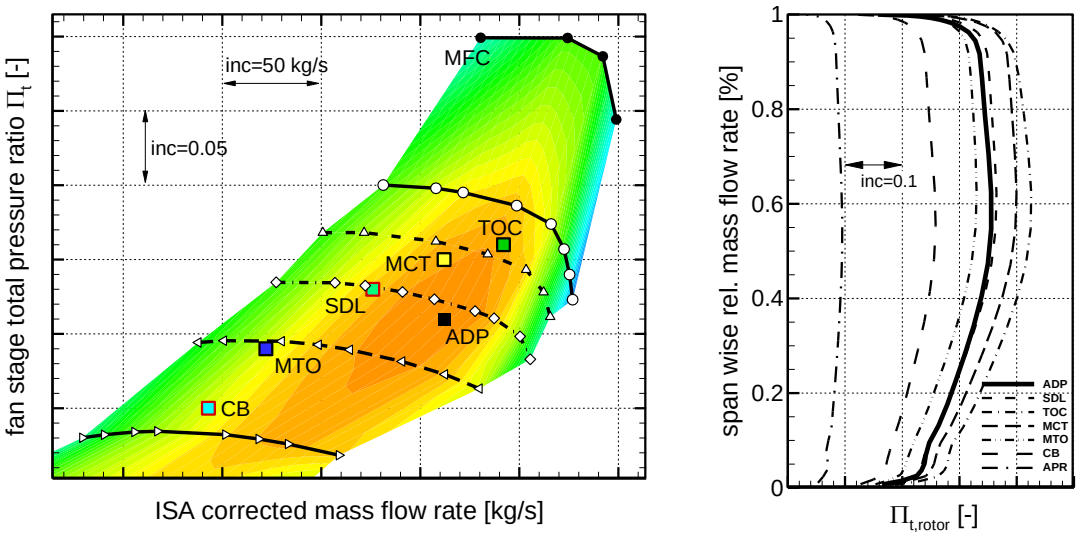

Figure 6 - Fan stage performance characteristics (left) and rotor total pressure ratio (right) over the entire flight envelope: Cruise (CR/ADP), Top of Climb (TOC), Sideline (SDL), Maximum Take-Off (MTO), Cutback (CB), Maximum Continuous (MCT) and Approach (APR) conditions – contours yield iso-isentropic efficiency with an increment of 0.25%

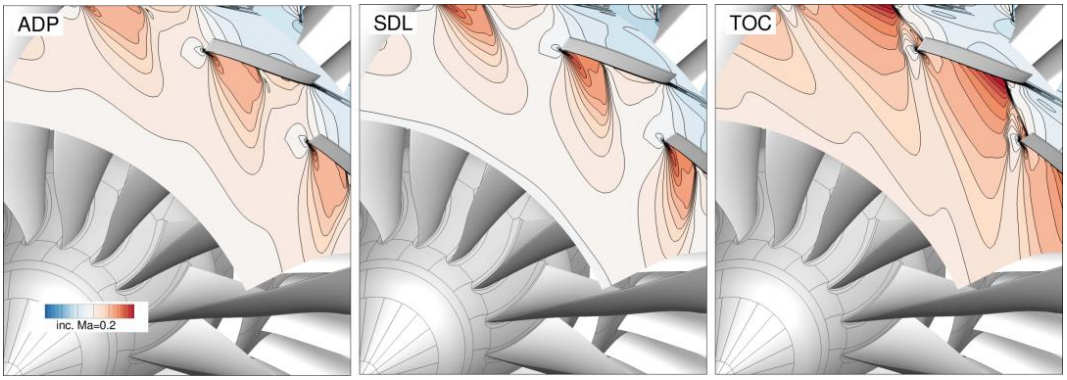

Figure 7 - Relative Mach number contours and iso-lines at 90% blade span at different operating conditions – results from steady state, single passage CFD computations of the isolated fan

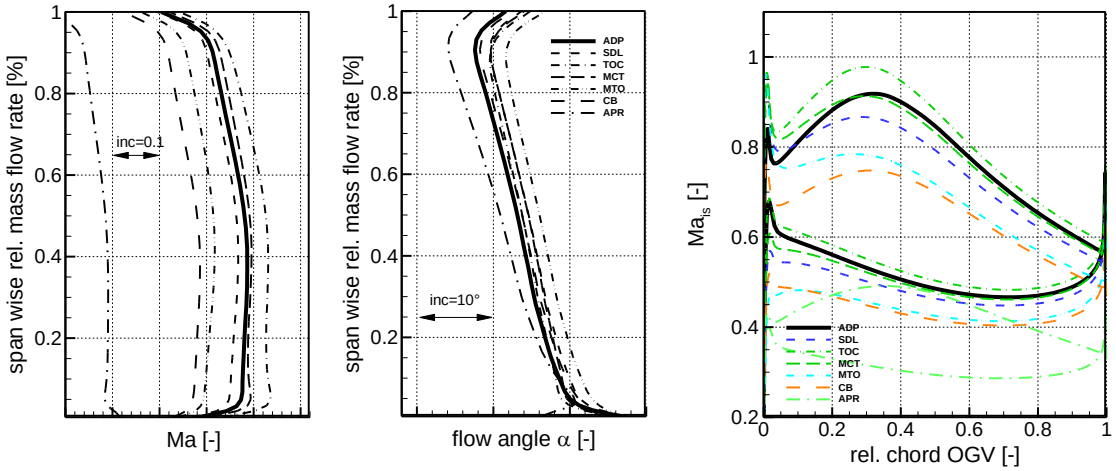

Figure 8 - Span-wise distribution of OGV inflow conditions (Mach number / left and flow angle / center) and isentropic Mach number distribution at OGV mid-span (right) in all relevant operating conditions

5.2 Fan and Intake

5.2.1 Cruise (ADP) and Sideline (SDL) Conditions

One of the first questions that came up after the design of the isolated propulsor was in how far the presence of the intake changes the average performance. To assess this first, of all steady state computations with the intake being added were compared with those of the isolated configuration. The results are shown in Figure 9 for SDL and ADP conditions. In the speedline shown in the left part of the figure one can observe how the characteristics deviate towards choke and the stability limit, whilst the design point itself was unaffected. In this case the choke mass flow rate was increased by 1.3% due to the presence of the intake. The reason for this can be explained by comparing the span wise distributions of axial velocity and local contraction in terms of the MVDR as shown in the right plots of Figure 9 for a position just upstream of the rotor leading edge. A difference in mass flow distribution radially can be observed, with lower values of axial velocity near the tip when the intake is present. This indicates a local diffusion and hence more positive distance to the passages operating at choked conditions. A better impression of the effect of the intake can be given when comparing the average axial velocity in a meridional view shown in Figure 10. Here the expansion region near the intake lip can be observed, which leads to an increase in axial velocity between 40 and 80% span. Also the local diffusion, caused by the convex curvature of the intake close to the leading edge, is visible in the vicinity of the casing. The discussed re-distribution of the mass flow has practically no effect on the total pressure ratio and resulting global performance of the fan stage.

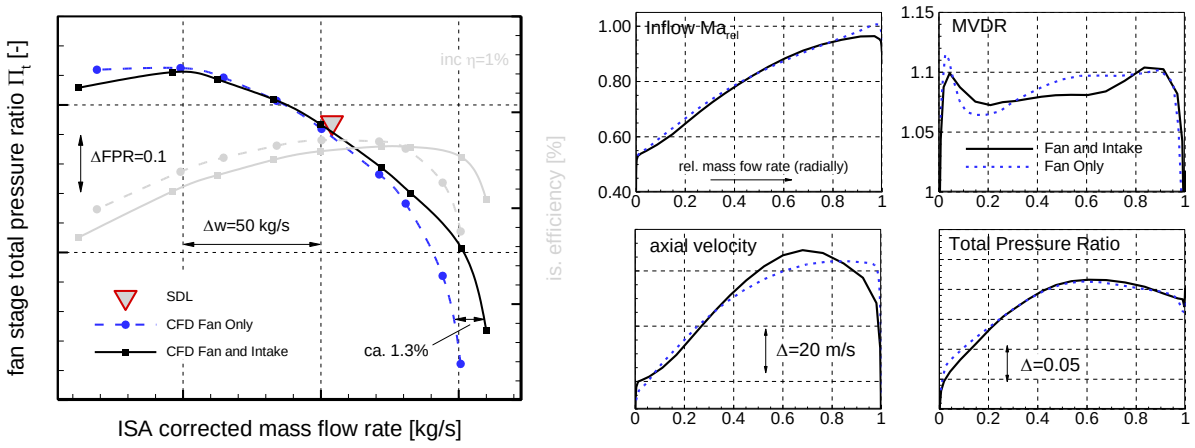

Figure 9 - Left: Influence of the presence of the intake on the initial design at the stage performance characteristics; Right: fan entry conditions and rotor performance parameters (circ. averaged) at SDL conditions over spanwise relative mass flow rate (blue dashed lines: isolated fan as designed – black solid lines: coupled fan and intake performance)

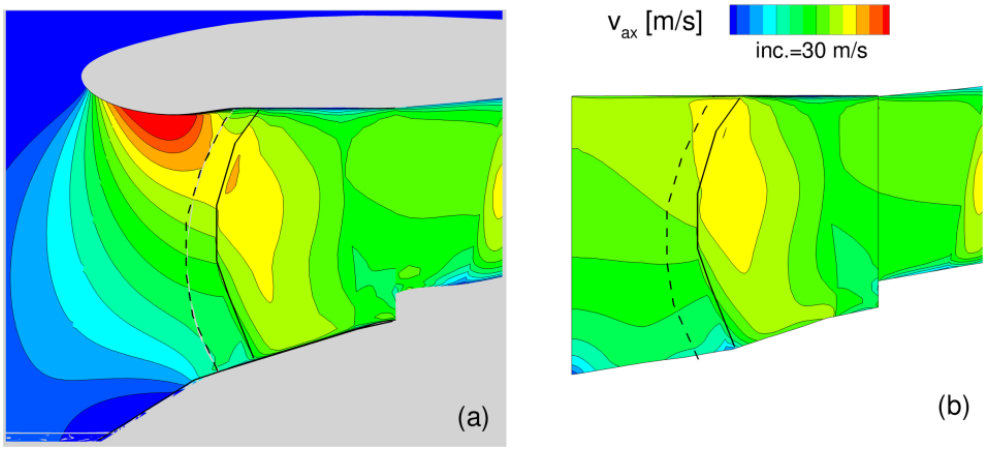

Figure 10 - Circumferentially averaged axial velocity resulting from steady state RANS computations with the intake present (a) and without the intake and constant tip radius upstream of the fan as used during the fan design (b) – SDL conditions

While adding the intake causes the aforementioned inclination of the characteristics due to a mass flow re-distribution compared with the isolated fan, a difference in Reynolds number almost constantly shifts the speed line over the entire working range as can be seen in Figure 11. Comparing the fan performance at different Re-levels is important when e.g. the overall design is done at ISA-SLS conditions, but the actual operation of the engine obviously takes place at altitude conditions, or when a different geometric scaling (full scale vs downscaled version for component tests) is being considered. The example shown in Figure 11 compares results for two different, chord-based Re-numbers which differ by a factor of 2-3 due to operation at Ma=0.87 in 35,000 ft compared with sea level static conditions (top left plot in right part of Figure 11). The resulting stage characteristics yield an approximate 1.5% decrease of efficiency and 0.05 in total pressure ratio for the lower Reynolds at altitude conditions; the radial distributions of the corresponding data at ADP, shown for the rotor only in the different plots in Figure 11 (right), show that only a portion of the overall performance degradation is caused in the rotor region with a decrease in efficiency by approximately 1% and only a very small change in rotor total pressure ratio. The remaining additional losses at low Re are being produced in the OGV's, which contribute with a rather high wetted area and resulting thicker boundary layer as well as larger regions of strong secondary flows, in particular near the hub. This can be seen qualitatively in Figure 12, where the corresponding S3-planes downstream of the rotor and the OGV are both shown in comparison for both Re numbers considered.

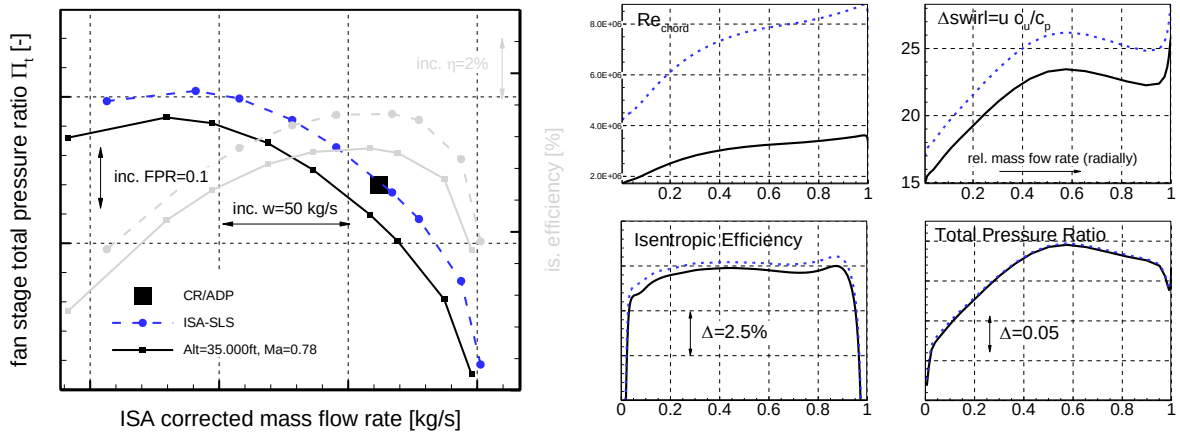

Figure 11 - Left: Stage performance characteristics at ISA-SLS and Cruise conditions; Right: rotor performance parameters (circ. averaged) at ADP over spanwise relative mass flow rate (black solid lines: Cruise conditions at 35,000 ft and flight Ma=0.78 / low Reynolds number – blue dashed lines: same values at ISA-SLS conditions / high Reynolds number)

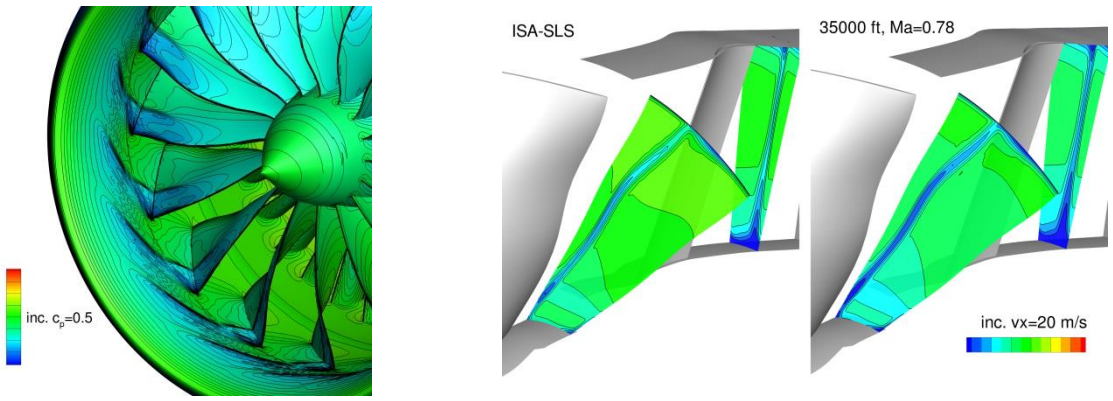

Figure 12 - Instantaneous contours of pressure coefficient cp (left) and rotor and OGV wakes and secondary flows at different Reynolds numbers (right)

All results discussed so far stem from steady state RANS computations with and without the intake being present and at axial inflow to the intake. In the next paragraphs, the unsteady interaction between a non-homogenous inflow, here caused by an angle of attack towards the intake at SDL conditions, and the fan shall be discussed. Different numerical approaches such as non-linear uRANS with phase shifted boundary conditions [24], as well as frequency based harmonic balance (HB) techniques [7], were being applied after having proven their respective applicability for those kind of scenarios [25].

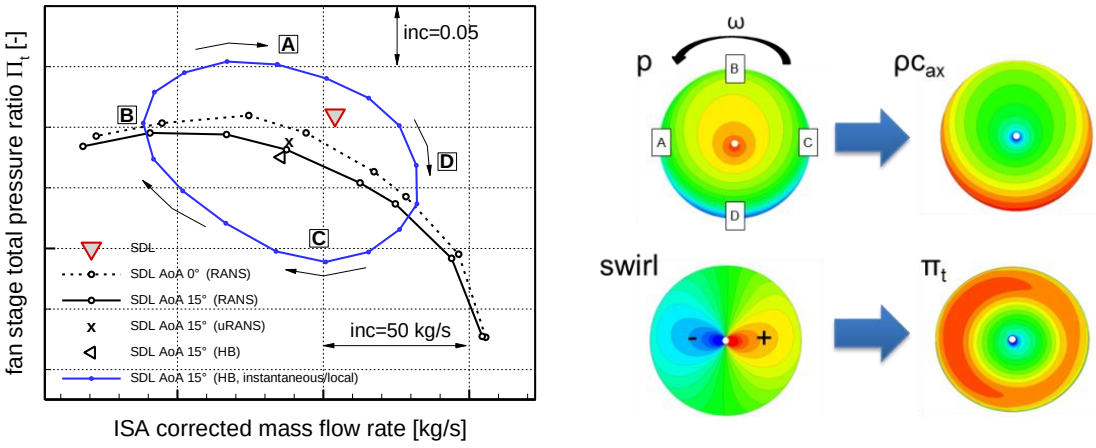

Figure 13 - Resulting excursions of the blade passage performance in the fan characteristics (left) and fan inlet conditions (p, ρcax and α) as well as resulting instantaneous fan total pressure ratio πt (right) – Results from steady state (SDL, AoA=0° and 15°) and uRANS/HB computations (SDL, AoA=15°). NB: Negative values of swirl indicate contra swirl and correspond to an increase of blade incidence and images are based on viewing the engine from the front)

Both unsteady methods yield very similar results as shown in the resulting performance characteristics in Figure 13 for the SDL point at 15° angle of attack. Shown in this figure is not only the SDL point itself as resulting from both methods, but also the steady state speed lines for axial inflow and 15° angle of attack (both having a mixing plane within the intake just upstream of the rotor as indicated by the dashed line in Figure 4). Apart from the shown time average performance metrics, the resulting excursions of the operating conditions of one individual blade passage as it moves along the circumference are also shown in this figure (the underlying stream-tube based post-processing to account for non-homogeneous inflow has been developed in [19]). Two regions with different flow features can be described: First of all regions A and C, located at 9 and 3 o'clock respectively (Figure

13, right). Both are dominated by simple kinematics, where the upward and downward movement of the blades relative to the flow incidence is inducing both, co- and contra swirl velocities. This co- and contra swirl essentially directly translates into an increase or decrease in total pressure ratio, without too much changing the local mass flow rate (lower right part in Figure 13). The nature of this interaction is visualized in Figure 14 by means of the pressure contours at the blade and intake surfaces. The predominant unsteady effect here is the change in the shock position, where counter swirl causes the shock to move upstream due to positive incidence and vice versa. Looking at the windward (D) and leeward (B) facing sections of the intake, the effects are different in nature and mainly cause an increase or decrease of the local mass flow rate at rather constant total pressure ratio levels. Here the larger expansion region at the windward facing part (D) of the intake lip increases the supersonic region in the front part of the blade with the shock moving downstream due to the higher inflow Mach number. No significant change in incidence could be observed and the local increase in mass flow density as shown in Figure 13 directly translates into a larger mass flow rate. The opposite effect can be observed at the leeward side (B) of the intake, where the diffusion reduces the local mass flow density. Comparing the shock systems on the leeward (B) and windward (D) side of the nacelle as sketched in Figure 15, one can see a diffusion on the upper part (B) of the nacelle intake with a reduction in mass flow density and a corresponding reduction in relative inflow Mach number, resulting in only a very small supersonic region with a weak shock in the front part of the blade profile. Due to the increased flow acceleration on the lower intake lip (windward side – D), this supersonic region is increased greatly with a stronger shock located further downstream to meet the imposed exit static pressure. In between all aforementioned regions, a smooth transition between those phenomena takes place, leading to the observed elliptical shape of the performance orbit. Finally, it can be summarized that the predominant unsteady interactions between the fan and the intake with distortions stemming from typical angle of attack conditions are different in nature as to compared with a generic sector distortion [6][19], ground vortex induced distortions [23], cross wind conditions [25] and a typical BLI scenario [8].

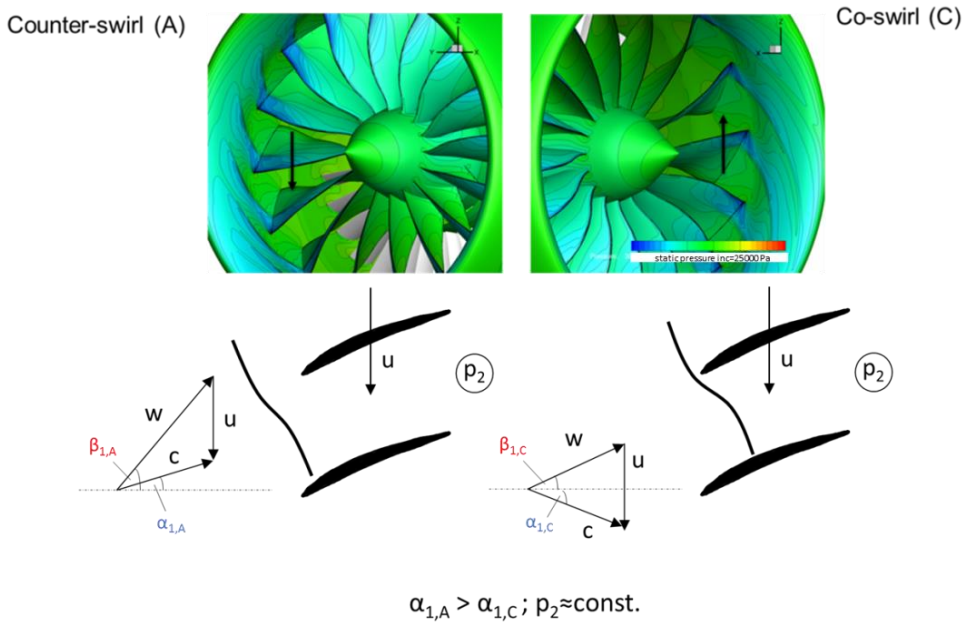

Figure 14 - Shock structure of the fan as being influenced by typical angle of attack conditions occurring during Take-Off (results at SDL conditions, AoA=15°) – blade downward (A) and upward (C) moving side of the nacelle intake

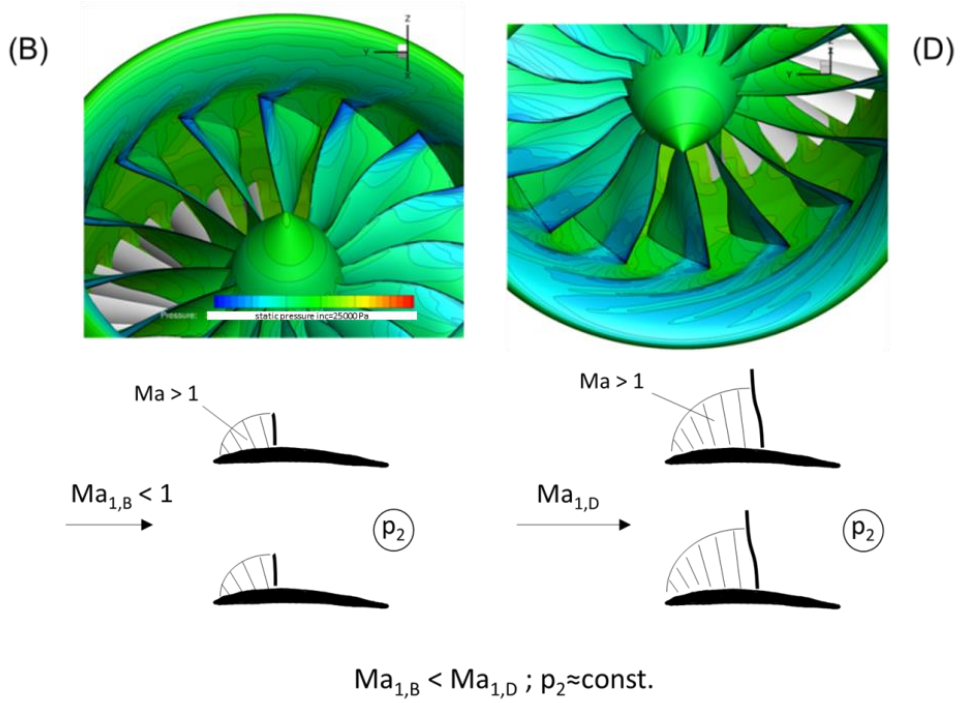

Figure 15 - Shock structure of the fan as being influenced by typical angle of attack conditions occurring during Take-Off (results at SDL conditions, AoA=15°) – windward (D) and leeward (B) view on the nacelle intake

5.2.2 Maximum Flow Capacity (MFC) at different angles of attack

As mentioned in the previous chapter, one important and often critical feature of any fan is its maximum achievable flow capacity. For this particular design, the values to be ensured were rather high and hence it was important to assess how the flow capacity changes and is potentially compromised at different angles of attack. This was investigated by means of harmonic balance (HB) computations, carried out at three different angles of attack. In all computations, the rotor RPM as well as the back pressure downstream of the OGV was kept constant. Results are shown in

Figure 16 in terms of contours of the pressure coefficient on the windward part of the intake and the lower half of the rotor. The increasing flow acceleration within the intake with increasing incidence can be observed with differences in the minimum cp of approximately Δcp~5 just upstream of the fan. Inside the rotor passage however the flow field is hardly affected and the passage shock stays at the very same position for all incidence angles and the additional acceleration is confined to the intake lip region. To further visualize this, the white dashed lines in all plots of

Figure 16 denote the shock position from the 15° reference case. In terms of resulting global values, a reduction in real mass flow rate wreal by more than 1% between the incidence free reference case (0°) and the maximum angle of attack of 25° was observed (see Figure 17). This was associated with an increase in intake losses by almost a factor of 3, which partly compensated for the reduction in reduced mass flow rate; here the difference between the reference case and maximum angle of attack was in the order of 0.5%. The stage efficiency levels were also affected by the (small) differences in shock strength, resulting in decreased stage efficiency by 1.5% for the maximum angle of attack (compared with the 0° reference). All the aforementioned effects on the fan choking characteristics need to be taken into account when defining the necessary margins and the results help quantifying these additional margins.

Finally, one aspect of the stall characteristics of the intake shall be further looked at. Only one example will be discussed here since the effect of the presence of the fan compared with a simple throughflow nacelle has been investigated already in previous studies [3] [27] and is well understood. In general, as shown in Figure 18, a separation occurring at the intake lip at extreme conditions can

be substantially delayed by the fan. The main reason is because the reduced static pressure associated with a potential separation is suppressed by the static pressure rise characteristic of the fan, which imposes a pressure from further downstream and the strong coupling of this pressure field with the intake diffusion. As shown in the result here, a fully separated intake at 30° angle of attack with massively separated regions within the nacelle (Figure 18, left), may, in a coupled fan and intake scenario, still operate reasonably well (Figure 18, right). Here a small separation within the intake and upstream of the fan is present, but not significantly compromises the fan performance and the blade passages are more or less free of separation. This needs to be considered not only when designing (short) intakes, but in particular when carrying out experiments with through flow nacelles.

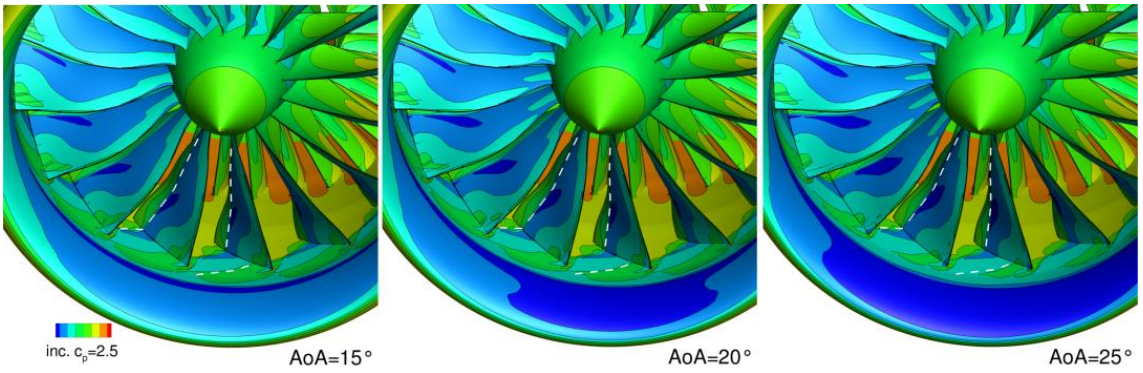

Figure 16 - Contours of the static pressure coefficient on the solid surfaces for three different angles of attack (shown is the windward side of the intake) – Results from HB computations

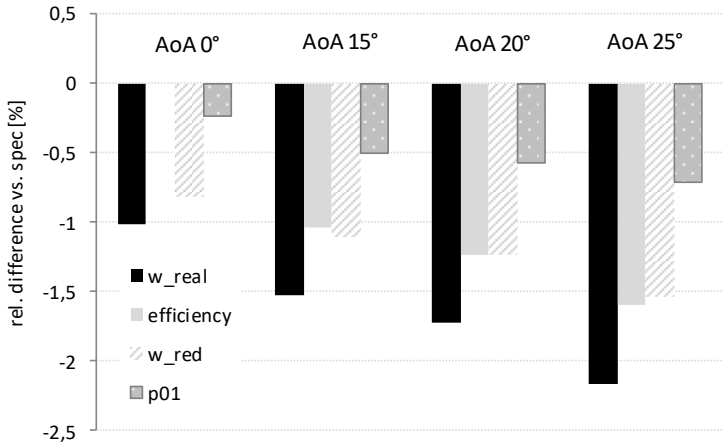

Figure 17 - Global fan stage performance data for difference angles of attack (average values from HB computations)

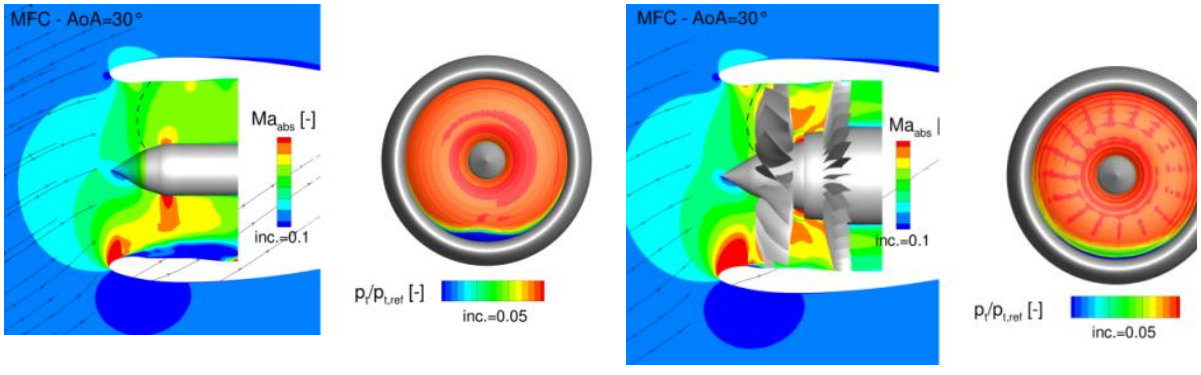

Figure 18 - Comparison of powered nacelle (with the fan present, right) and non-powered nacelle (without the fan, left) at operating conditions near maximum flow capacity (MFC) and 30° angle of attack

6. CONCLUSIONS AND OUTLOOK

The paper documents the design and performance assessment of a low fan pressure ratio propulsion system aiming at bypass ratios of 16 and beyond from the conceptual design phase to the full CFD assessment of the integrated fan with the nacelle and intake being present. Several operational and performance related aspects of the fan and intake design were considered and in this context it was quantified how the presence of the intake affected the fan performance at different flight conditions. This propulsion system has already been extensively used in the European research community as a test case for code benchmark of installed propulsions systems with extremely short intake aiming at overall aerodynamic performance [13] as well as dedicated investigations regarding special topics of interest in fan aerodynamics such as fan blade transition [16], and to provide a deeper understanding of the effect of non-axisymmetric inflow to fan tonal noise emissions [9][11][17]. The propulsion system and in particular the fan design as described in this paper will also be the basis to derive a scaled version of the fan module for experimental investigations of a representative UHBR engine installation in low and high speed wind tunnels (see Figure 19).

Figure 19 - SA²FIR Installation Rig from Clean Sky Initiative LPA[1] (left) and intake acoustic resonance flutter sensitivity study exploiting the test rig taken from [29]

ACKNOWLEDGMENTS

This project has received funding from the Clean Sky 2 Joint Undertaking under the European Union's Horizon 2020 research and innovation program under grant agreement No 681856 – ASPIRE.

Smaller parts of this project have received funding from the Clean Sky 2 Joint Undertaking (JU) under grant agreement No. 945583. The JU receives support from the European Union's Horizon 2020 research and innovation programme and the Clean Sky 2 JU members other than the Union.

[1] from: https://cleansky.virtualfair.be/hangar

Copyright Statement

NOMENCLATURE

Acronyms	
ADP	Aerodynamic Design Points
AoA	Angle of attack
APR	Approach
CR	Cruise
DF	Lieblein Diffusion Number
FPR	Fan pressure ratio
MTO	Maximum Take-Off
MFC	Maximum Flow Capacity
MVDR	Meriodional Velocity-Density-Ratio
SDL	Sideline
SLS	Sea Level Static
OGV	Outlet Guide Vane
TOC	Top of Climb

Symbols	
α, β	Flow angle (absolute, relative)
δ	Air intake drop angle
Ψ	Work coefficient
φ	Flow coefficient = v_x / u_{mean}
ν	Rotor hub-to-tip ratio
η	Isentropic efficiency
π	Pressure ratio
ρ	Density
c	Velocity
c_p	Pressure coefficient = $(p-p_\infty)/ (\rho v_\infty^2)$
D	Fan casing diameter
L	Intake length (between fan blade root leading edge and intersection between intake highlight plane and engine axis)
p	Pressure
T	Temperature
u	Velocity
w	(reduced) Mass flow rate

Subscripts

0	(Inlet) stagnation quantity
ff	Fan face
is	Isentropic
mean	Reference (mid-area)
red	(ISA) reduced
u	Circumferential velocity component (absolute)
1,2	Blade row inlet, outlet
t	Total
tip	Blade tip
∞	Free stream values far upstream the fan / flight conditions

References

[1] Bewick, C.L., Adams, M.J., Schwaller, P.J.G., Xu, L.: *Noise and Aerodynamik Design and Test of a Low Tip Speed Fan*, AIAA-2001-2268, 7th AIAA/CEAS Aeroacoustics Conference, Masstricht, The Netherlands, 2001

[2] Burlot, A., Sartor, F., Vergez, M., Méheut, M., Barrier, R.: *Method Comparison for Fan Performance in Short Intake Nacelle*, Applied Aerodynamics Conference, AIAA AVIATION Forum, AIAA 2018-4204, https://doi.org/10.2514/6.2018-4204, 2018

[3] Carnevale, M., Wang, F., di Mare, L: *Low Frequency Distortion in Civil Aero-engine Intake*, Journal of Engineering for Gas Turbines and Power, APRIL 2017, Vol. 139 / 041203-1, 2017

[4] Crichton, D., Xu, L., Hall, C.A.: *Preliminary Fan Design for a Silent Aircraft*, Journal of Turbomachinery 184 / Vol. 129, 2007b, pp. 184-191, January 2007

[5] Envia. E., Kerschen, E.: *Influence of Vane Sweep on Rotor-Stator Interaction Noise*, NASA Contractor Report 187052, 1990

[6] Fidalgo, V. J., Hall, C. A., and Colin, Y., 2010. "*A Study of Fan-Distortion Interaction within the NASA Rotor 67 Transonic Stage*". In Proceedings of ASME Turbo Expo, Glasgow, UK, GT2010-22914

[7] Frey, C., Ashcroft, G., Kersken, H.-P., Schoenweitz, D., and Mennicken, M., 2017. "*Simulation of Indexing and Clocking with Harmonic Balance*". International Journal of Turbomachinery, Propulsion and Power 3 (1), Multidisciplinary Digital Publishing Institute (MDPI) DOI: 10.3390/ijtpp3010001 ISSN 2504-186X.

[8] Gunn, E. J., and Hall, C. A., 2014. "*Aerodynamics of Boundary Layer Ingesting Fans*". In Proceedings of ASME Turbo Expo, Duesseldorf, Germany, GT2014-26142

[9] Guerin, S., Holewa, A.: *Fan tonal noise from aircraft aero engines with short intake: a study at approach*, 21st Workshop of the Aeroacoustics Specialists Committee of the CEAS, Trinity College Dublin, 13-15.09.2017, also to be published at International Journal of Aeroacoustics

[10] Jaron, R.: *Aeroacoustic Design of Aeroengine Fans by means of Multidisciplinary Optimizations*, DLR Forschungsbericht FB-2018-21 (german language, also PhD Thesis at TU Berlin), Berlin 2018

[11] Laban, M., Kok, J.C. and Brouwer, H.H.: *CFD/CAA Analysis of UHBR Engine Tonal Noise*, AIAA Aviation and Aeronautics Forum and Exposition (AIAA AVIATION 2018), 25-29 June 2018, Atlanta/GA, USA

[12] Lengyel, T., Voß, C., Nicke, Rüd, K.-P., Schaber, R.: *Generalized Optimization of Counter-Rotating and Single-Rotating Fans*, ASME Paper No. GT2014-26008, pp. V01AT01A022; 13 pages, ASME Turbo Expo 2014: Turbine Technical Conference and Exposition, doi:10.1115/GT2014-26008, Düsseldorf, Germany, June 16–20, 2014

[13] Meheut, M., Sartor, F., Vergez, M., Laban, M., Schnell, R. Stürmer, A.: *Assessment of Fan/Airframe aerodynamic performance using 360° uRANS computations: Code-to-Code comparison between ONERA, DLR and NLR*, Paper ID 3030873, AIAA SciTech Forum, 2019

[14] Meillard, L., Ben Nasr, N., Stanica, C., Riéra, W.: *Multidisciplinary design optimization of a counter rotating fan under high level of restriction*, ISABE-Paper 2017- 21387, 23st ISABE Conference, 9.-13. September, Manchester/UK, 2017

[15] Moyon, F., Wilson, M., Schnell, R. *Low Pressure Ratio Fan Design – Challenges, Fan Design Strategy and Results for UHBR Engines*, Paper #0116, Greener Aviation Conference, Brussels, 11-13 October 2016

[16] Pascal, L., Barrier, R., Billonet, G., Marty, J.: *Linear stability analysis in rotating frames and its application to fan blade transition prediction*, AIAA Aviation and Aeronautics Forum and Exposition (AIAA AVIATION 2018), 25-29 June 2018, Atlanta/GA, USA

[17] Polacsek, C., Chelius, A., Daroukh, M., François, B., Barrier, R.: *TONE NOISE PREDICTION OF A FULL-SCALE UHBR ENGINE WITH SHORT INLET AND INFLOW DISTORTION*, 25th International Congress on Sound and Vibration, 8-12 July, Hiroshima/Japan

[18] Schnell, R. Giebmanns, A., Nicke, E., Dabrock, T.: *AERODYNAMIC ANALYSIS OF A FAN FOR FUTURE ULTRA-HIGH-BYPASS-RATIO AERO ENGINES*, ISABE Paper 2009-1149, 19th ISABE Conference, September 7-11-2009, Montreal/Canada

[19] Schoenweitz, D., Theune, M., Schnell, R.: *Inlet Distortion Sensitivity of Fans with Different Pressure Ratios*, ISABE Paper ISABE-2015-22008, 22nd ISABE Conference (International Society for Air Breathing), September 2015, Phoenix/AZ, USA

[20] Schoenweitz, D., Schnell, R.: *Development and Evaluation of a Performance Estimation Methodology for Fans Operating within non-homogeneous Inflow*, ASME Paper GT2017-57095, ASME Turbo Expo Seoul/Korea, 2016

[21] Schnoes, M., Voß, C., Nicke, E.: *Design Optimization of a Multi-Stage Axial Compressor using Throughflow and a Database of Optimal Airfoils*, GPPS-2018-0009, Proceedings of Montreal 2018 Global Power and Propulsion Forum 7th - 9th May, 2018

[22] Schuff, M., Reisberg, J.: *FLUTTER ANALYSIS OF A FLEXIBLE UHBR FAN AT DIFFERENT FLIGHT CONDITIONS*, ASME Paper GT2018-76930, Proceedings of the ASME Turbo Expo 2018, June 11-15, Oslo/Norway

[23] Schoenweitz, D., Becker, R.-G., Schnell, R., Schroll, M: *Aerodynamic Performance Characteristics of the Installed V2527 Fan at Ground Operation*, American Institute of Aeronautics and Astronautics Conference and Proceedings, January 2016

[24] Schnell, R.: *Investigation of the Acoustic Nearfield of a Transonic-Fanstage by Time-Domain CFD-Calculations with Arbitrary Blade Counts.* ASME Paper GT2004-54216, ASME Turbo-Expo 2004, 7.-14. Juni 2004, Wien/Österreich, ASME, (2004)

[25] Schnell, R., Corroyer, J.: *Coupled Fan and Intake Design Optimization for Installed UHBR-Engines with Ultra-Short Nacelles*, 23rd International Symposium on Air Breathing Engines ISABE 2015 Phoenix/AZ, USA

[26] Stuermer, A.: *Assessing Turbofan Modeling Approaches in the DLR TAU-Code for Aircraft Aerodynamics Investigations*", AIAA Scitech 2019 Forum, AIAA SciTech Forum, (AIAA 2019-0277), https://doi.org/10.2514/6.2019-0277, 2019

[27] Thollet, W., Dufour, G., and Carbonneau, X., 2016. "*Assessment of body force methodologies for the analysis of intake-fan aerodynamic interactions"*. In Proceedings of ASME Turbo Expo 2016.

[28] C. Klein; F. Wolters; S. Reitenbach; D. Schönweitz: *Integration of 3D-CFD Component Simulation Into Overall Engine Performance Analysis for Engine Condition Monitoring Purposes*, Proc. ASME. 50985; Volume 1: Aircraft Engine; Fans and Blowers; Marine, V001T01A013.June 11, ASME Paper GT2018-75719 doi: 10.1115/GT2018-75719, 2018

[29] Schnell, R., Frey, C.: *Acoustic Impact on Fan Flutter in Short Aero Engine Intakes*, Proceedings AIAA Aviation Forum 2021 August 02-06, Washington/DC, US